Journal of Nuclear Materials 404 (2010) 210–216

Contents lists available at ScienceDirect

Journal of Nuclear Materials

journal homepage: www.elsevier.com/locate/jnucmat

Densification of nano-CeO_2 ceramics as nuclear oxide surrogate by spark plasma sintering

Kwanghoon Choi [a], Wen Tong [a], Robert D. Maiani [b], Douglas E. Burkes [c], Zuhair A. Munir [a,*]

[a] Department of Chemical Engineering and Materials Science, University of California, Davis, CA 95616, United States
[b] Materials and Fuels, Idaho National Laboratory, Idaho Falls, ID 83415, United States
[c] National Nuclear Security Administration, Washington, DC 20585, United States

ARTICLE INFO

Article history:
Received 12 March 2010
Accepted 8 July 2010

ABSTRACT

The sintering and resulting microstructure of nano-grained CeO_2 ceramics were investigated as functions of the spark plasma sintering (SPS) parameters. Ceria powders could be sintered to a relative density over 97% with a grain size of about 30 nm. The applied uniaxial pressure during sintering had a significant effect on densification. The combination of high pressure and fast heating rate produces a marked reduction in the sintering temperature to densify CeO_2 with very limited grain growth. Heating rate and holding time, however, had insignificant effect on density but a measurable effect on grain size.

© 2010 Elsevier B.V. All rights reserved.

1. Introduction

In contrast to zirconia, ceria (CeO_2) is stable in the cubic fluorite structure from room temperature to its melting point (~2750 K). It is an important ceramic for various applications such as electrolyte in solid oxide fuel cells (SOFC) [1], oxygen sensor material [2], catalytic support [3], and as oxygen storage capacity material in automobile exhaust systems [4]. It has also been investigated as surrogate material for plutonium oxide in mixed oxide (MOX) fuels since its properties are similar to those of PuO_2 [5,6]. Also, its use as a surrogate has the advantages of well-established synthesis methods, good resistance to radiation damage, and compatibility with reactant coolant [7].

The sintering of pure and doped CeO_2 has been investigated on powders synthesized by various methods. Chen and Chen [8] prepared ceria by a precipitation method and showed that the powders could be sintered to near full density at 1250 °C in 6 min. No information on the grain size was reported, but an estimate of the size could be made from the micrograph provided in this paper as roughly 1 μm. Using an electrochemical method of preparation, Zhou et al. [9] synthesized powders with an average grain size in the range 10–14 nm. Samples having a density of 99.8% and grain size of 0.35 μm were obtained by sintering at 1300 °C for 2 h. Undoped ceria was also prepared by a polymeric organic complex method with the smallest grain size being in the range 8–12 nm [10]. The sintering temperature and the density and grain size of samples made by variations in this method depended on the degree of agglomeration of the powders. Powders with low agglomeration could be sintered at 1250 °C for 10 h to produce samples with a density of ⩾98% and an unspecified sub-micrometer grain size. Higher temperatures are required to densify powders with a higher degree of agglomeration [10].

In the most recent study on the sintering nanometric ceria powders, Kinemuchi and Watari [11] showed a dependence of the final density on the green density of the samples. But the density of their consolidated samples did not exceed about 90%, regardless of the initial green density. These authors also reported a bimodal shrinkage behavior for nanopowders, in agreement with prior observations by Zhou and Rahaman [12] and Ozawa [13]. In the former it was concluded that ceria released oxygen above 1200 °C and in the latter it was reported that two temperature ranges exist for this phenomenon, 700–800 °C and >1600 °C. In both studies, it was concluded that sintering is enhanced by the loss of oxygen, i.e., by

$$CeO_2 = CeO_{2-x} + (x/2)O_2 \quad (1)$$

$$xO_o = xV_o^{\cdot\cdot} + 2xe + (x/2)O_2 \quad (2)$$

where the Kröger–Vink symbols $V_o^{\cdot\cdot}$ and O_o represent a doubly charged oxygen vacancy, and oxygen on its sublattice, respectively.

In Ozawa's work [13], the occurrence of a higher shrinkage rate concomitantly with the loss of oxygen at low temperatures (700–800 °C) was observed only in the sintering of nanometric powders. Observation similar to that of Ozawa has been reported when ceria is used in catalysis [14], two peaks of oxygen release were reported, at 500 and 750 °C, and were attributed to reduction of surface and bulk oxide, respectively. Kinemuchi and Watari reached the same conclusion, except that the reduction at these two locations takes place at different temperatures, depending on the green density of the nanopowder sample. It was suggested that oxygen

* Corresponding author.
E-mail address: zamunir@ucdavis.edu (Z.A. Munir).

0022-3115/$ - see front matter © 2010 Elsevier B.V. All rights reserved.
doi:10.1016/j.jnucmat.2010.07.018

vacancies resulting from the loss of O_2 enhance grain boundary diffusion and hence densification.

In all of the studies referred to above, sintering was carried out by conventional methods and the samples needed to be heated to a minimum temperature of 1000 °C to achieve high densities (>95%). At this and higher sintering temperatures, the samples exhibited considerable grain growth with the smallest grain size being in the sub-micrometer range (0.35 μm) [9]. Generally similar results were obtained with yttria-, and gadolinia-doped ceria when conventional sintering methods were used [15,16]. In a more recent study, Mori et al. [17] investigated the sintering of dysprosia-doped ceria by conventional and spark plasma sintering (SPS) methods and found that a combination of these two methods gave the best results: 95+% dense samples with a grain size of <300 nm were obtained.

In contrast, Anselmi-Tamburini et al. [18], using a high pressure modification of the SPS method and starting with nanopowders (~8 nm), were successful in sintering pure and samaria-doped ceria to densities of >98% and with grain sizes of about 12 and 17 nm, respectively. In this work we investigate systematically the sintering of pure ceria as a function of the SPS parameters of temperature, pressure, heating rate, and dwell time.

2. Experimental materials and methods

The spark plasma sintering method has been used extensively in the past few years because of demonstrated advantages over conventional sintering methods. A detailed description of the method and examples of recent investigations utilizing it are given in a recent review [19]. We utilized this method in the present study using a Sumitomo Coal Mining Co., Model 2050 SPS apparatus. A schematic of the apparatus is shown in Fig. 1. We utilized a pulsing pattern of 12-2, i.e., 12 pulses on and 2 pulses off. Each pulse has a duration of 3.3 ms. In order to apply very high pressures, we developed a double-acting die, a schematic diagram of which is shown in Fig. 2. With this device we can routinely achieve pressures from 400 to 700 MPa and up to 1 GPa on a sample 5 mm in diameter and around 1.5 mm thick, while maintaining the ability of fast heating rates. The device is composed of an external graphite die, very similar in shape to a traditional SPS die. Two protective discs of pure, fully-dense tungsten carbide are placed at the end of each plunger. The low-pressure (outer) section of the die was made out of high-density graphite, while the high pressure (inner) section was made out of silicon carbide and tungsten carbide. Temperatures were measured using a shielded K-type thermocouple inserted in the lateral wall of the external die. The actual sample temperature was determined through a calibration. The calibration involved placing a second thermocouple in the center of the samples and establishing a calibration curve that covers the ranges of temperature and pressure used in this study.

High purity commercial nano-sized CeO_2 (Aldrich Chemical Co., 99.9% pure) was used as the starting materials. The particle size of

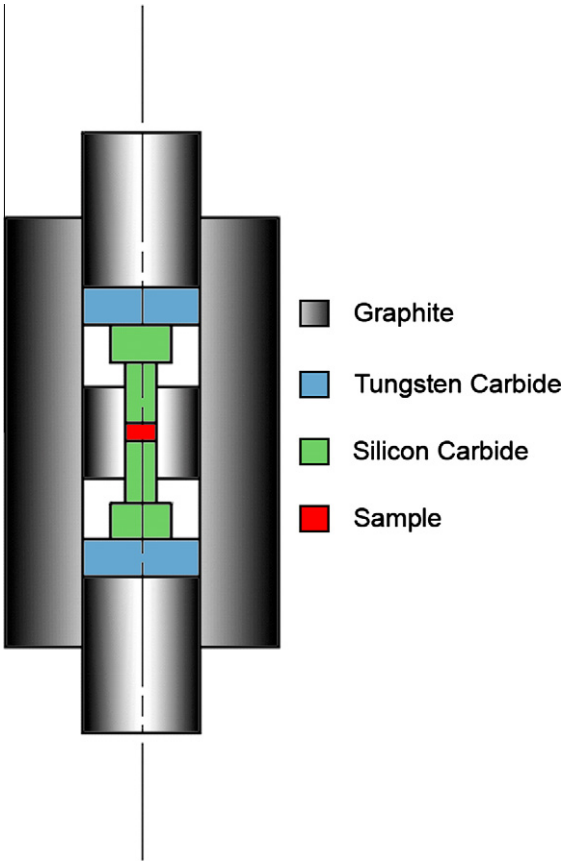

Fig. 2. Schematic of a double-acting die for high-pressure sintering in the SPS.

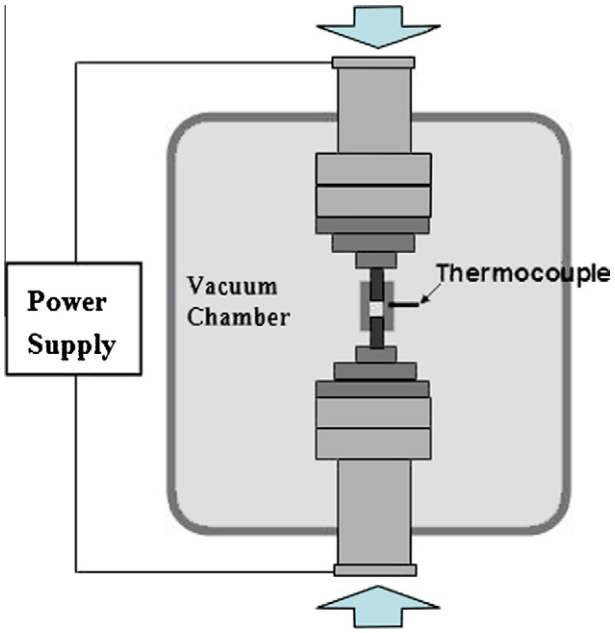

Fig. 1. Schematic diagram of the spark plasma sintering (SPS) apparatus.

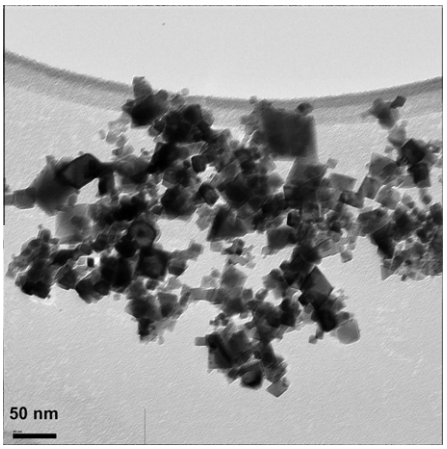

Fig. 3. TEM image of commercial nano-CeO_2 powder.

Table 1
SPS conditions, relative density, and grain size of sintered CeO_2.

Material	Starting powder grain size (nm)	Temperature range (°C)	Pressure range (MPa)	Heating rate range (°C min^{-1})	Holding time range (min)	Relative density (%)	Grain size (nm)
CeO_2	25	650–700	500	130	5	~97	28–54
		650–700	400–700	130	5	93–98	40–63
		780	400	78–330	2	~98	88–113
		780	400	130	0–10	~98	104–263

this powder is about 25 nm as can be seen by the TEM image of Fig. 3. About 0.15 g of powders were poured into a double stage die, and pressed under a pressure of 150 MPa before heating. The sintering process was investigated as a function of temperature, pressure, heating rate, and holding time. The sintering temperature was in the range 650–780 °C and the applied pressure ranged from 400 to 700 MPa. The temperature was increased linearly using heating rates ranging from 90 to 330 °C min^{-1}. The pressure was rapidly increased to its final value before reaching the final sintering temperature. The holding time was varied from 0 to 10 min. Table 1 shows the SPS parameters, relative density, and grain size of the sintered samples.

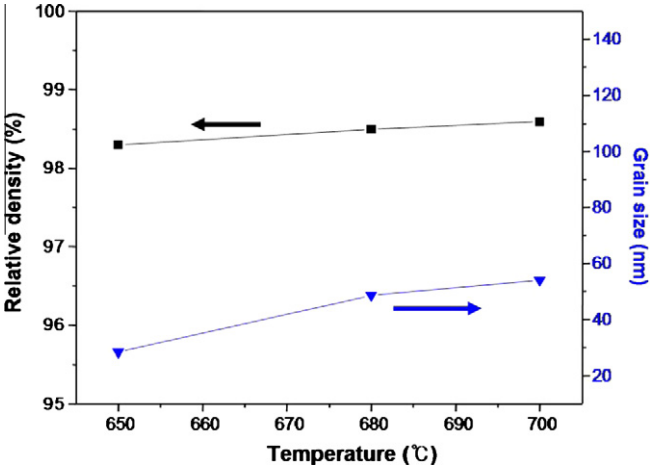

Fig. 4. Temperature dependence of relative density and grain size of CeO_2 at constant pressure (500 MPa), heating rate (130 °C min^{-1}), and holding time (5 min).

The density of the sintered samples was determined by the Archimedes method. The grain size in sintered samples was determined from SEM observations on fracture surfaces (Philips FEI XL-30). The grain size was determined from at least 100 grains using the software AnalySIS (Soft Imaging System Corp., Lakewood, CO). X-ray diffraction (XRD) was used to identify the phases and to also calculate the grain size by the Williamson–Hall method [20]. XRD was performed using Scintag XDS 2000 X-ray powder diffractometer.

3. Results and discussion

The effect of sintering temperature on the relative density and grain size of ceria is shown in Fig. 4. The samples were sintered at the indicated temperatures for 5 min under a uniaxial pressure of 500 MPa. The heating rate was 130 °C min^{-1} for all cases. For all samples, the density was high, exceeding 98% even for those sintered at the lowest temperature, 650 °C. Such a high density was not obtained in previous studies unless sintering was carried out at much higher temperatures. In the study by Zhou and Rahaman, powders with an approximate grain size of 25 nm required

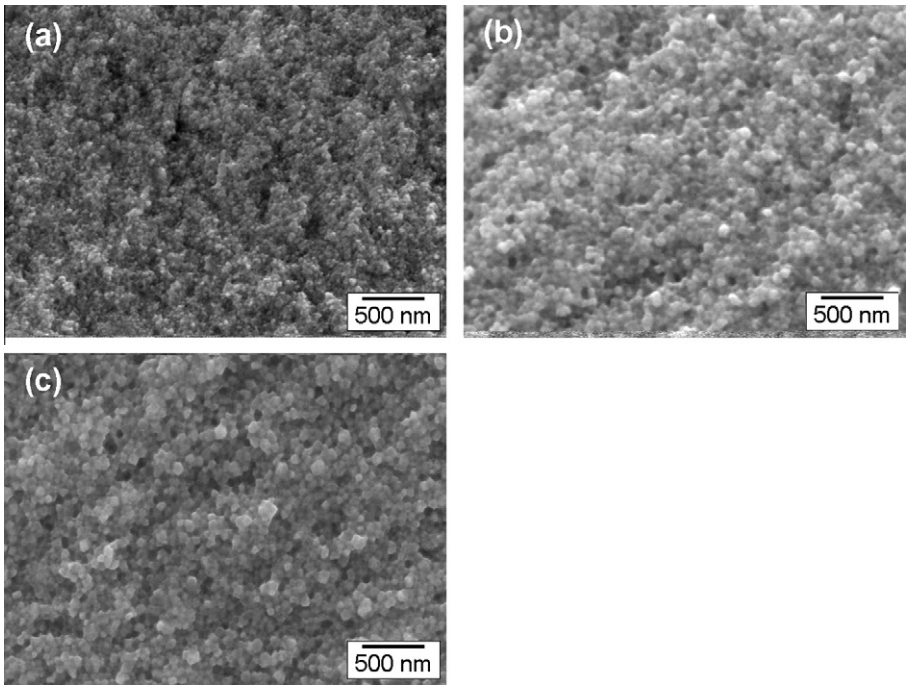

Fig. 5. SEM images of fracture surfaces of CeO_2 sintered at different temperatures: (a) 650, (b) 680 and (c) 700 °C (pressure: 500 MPa; heating rate: 130 °C min^{-1}; holding time: 5 min).

a sintering temperature of about 1150 °C to achieve a density of about 95% [12]. And similarly in the study by Duran et al. to achieve a density of 98%, samples had to be sintered at 1250 °C for 10 h [10]. As can be seen from Fig. 4, an increase in temperature (from 650 to 700 °C) had a small effect on density. However, it had a significant effect on grain size, which increased from about 27 to 55 nm. The grain size values plotted in Fig. 4 were determined from measurements on SEM images of fracture surfaces of samples sintered in this range, Fig. 5.

In the present work, the combination of fast heating rate and high pressure produces a marked reduction in the sintering temperature, as we reported in the cited earlier study on yttria-stablized zirconia [18]. Faster heating rates have been shown to enhance densification by by-passing the non-densifying mecha-

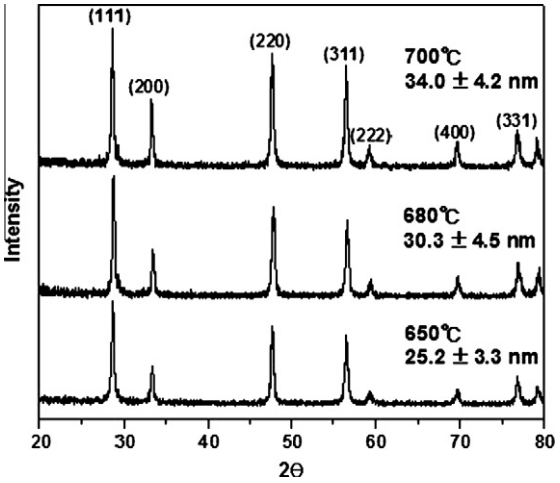

Fig. 6. XRD patterns of CeO_2 samples sintered at different temperatures (pressure: 500 MPa; heating rate: 130 °C min^{-1}; holding time: 5 min). Numbers indicate grain sizes calculated from line-broadening.

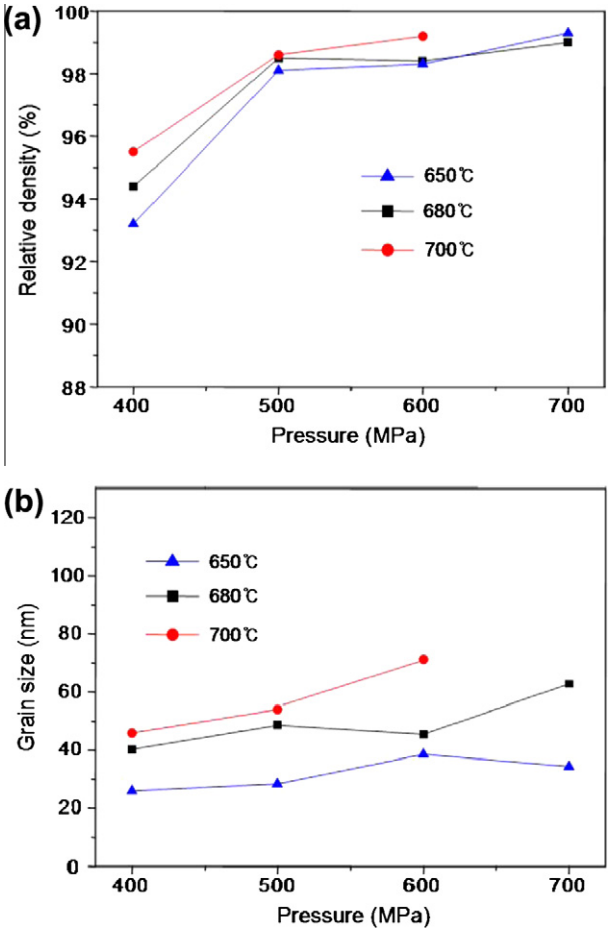

Fig. 7. Effect of pressure on relative density and grain size of CeO_2 sintered at constant temperature (680 °C), heating rate (130 °C min^{-1}), and holding time (5 min): (a) relative density and (b) grain size.

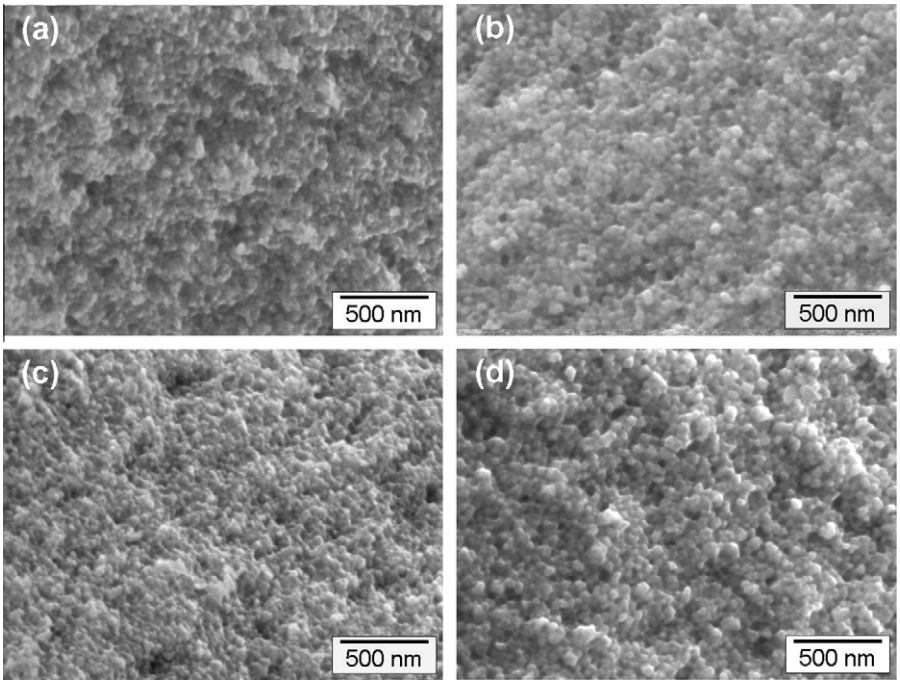

Fig. 8. SEM images of fracture surfaces of CeO_2 sintered at 680 °C under different pressures: (a) 400, (b) 500, (c) 600, and (d) 700 MPa (heating rate: 130 °C min^{-1}; holding time: 5 min).

nism of surface diffusion and by creating an additional driving force due to large thermal gradients [21]. When powders are sintered under a high applied pressure, greater densification is achieved at a constant temperature. There are numerous examples based on the use of hot-pressing investigations [22]. The pressure has a mechanical role as well as an intrinsic role. Mechanically the pressure has a direct effect on particle re-arrangement and the destruction of agglomerates, particularly in the case of nanometric powders.

The grain size was also calculated from XRD patterns shown in Fig. 6, using the Williamson–Hall method [20]. The calculated values are indicated on the patterns of the figure. These values, ranging from about 25 to 34 nm as the sintering temperature was increased from 650 to 700 °C, are lower than those obtained from SEM measurements. When compared with the grain size of the initial (unsintered) powder, these results show very limited grain growth during the sintering to obtain high densities under the SPS conditions.

The effect of applied pressure on the density and grain size was investigated. Fig. 7a shows the effect on density and Fig. 7b shows the effect on grain size at the three sintering temperatures. The relative density increased with increasing applied pressure over the temperature range 650–700 °C, with the most significant increase occurring between 400 and 500 MPa. These results clearly show that the pressure has a significant effect on densification at constant temperature, thus making possible the goal of achieving smaller grain size in dense samples. Similar observations were seen in the SPS sintering of nanopowders of yttria-stabilized zirconia [18]. As indicated above, the pressure can have an extrinsic influence (e.g., particle re-arrangement and break up of agglomer-

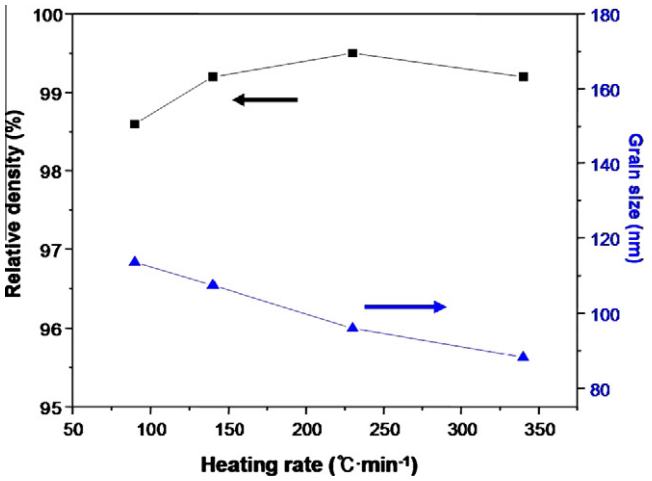

Fig. 9. Effect of heating rate on relative density and grain size of CeO_2 sintered at constant temperature (780 °C), pressure (400 MPa), and holding time (2 min).

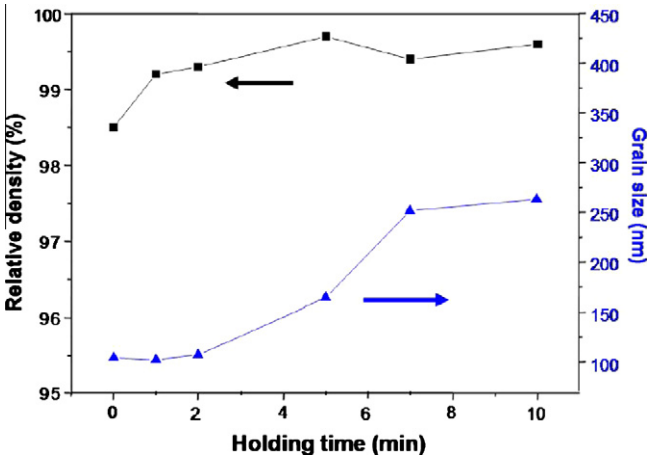

Fig. 11. The effect of holding time on relative density and grain size of CeO_2 (temperature: 780 °C; pressure: 400 MPa; heating rate: 140 °C min^{-1}).

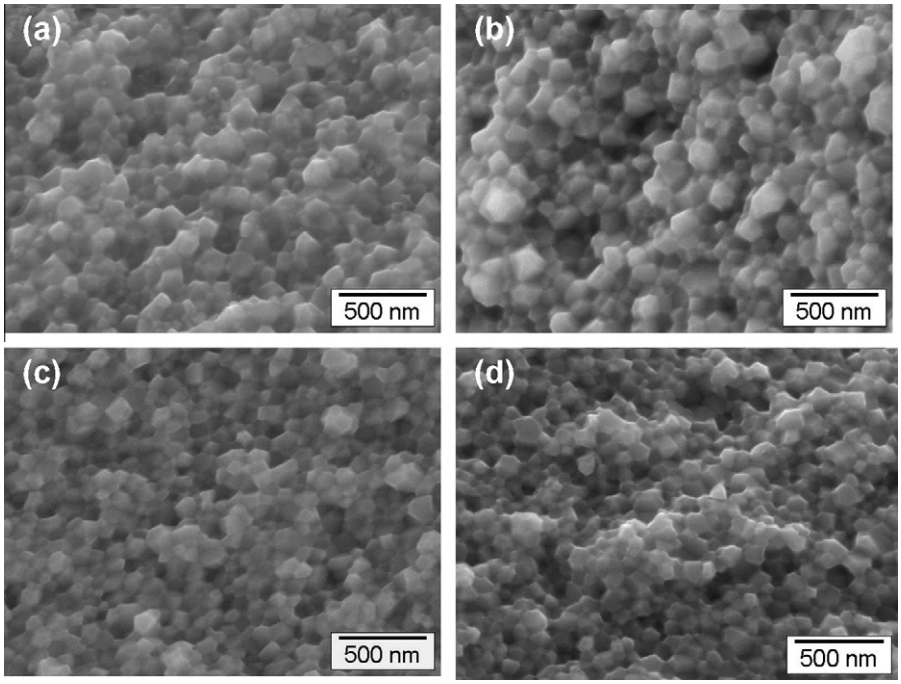

Fig. 10. SEM images of fracture surfaces of CeO_2 sintered at different heating rates: (a) 90, (b) 130, (c) 230, and (d) 330 °C min^{-1} (temperature: 780 °C; pressure: 400 MPa; holding time: 2 min).

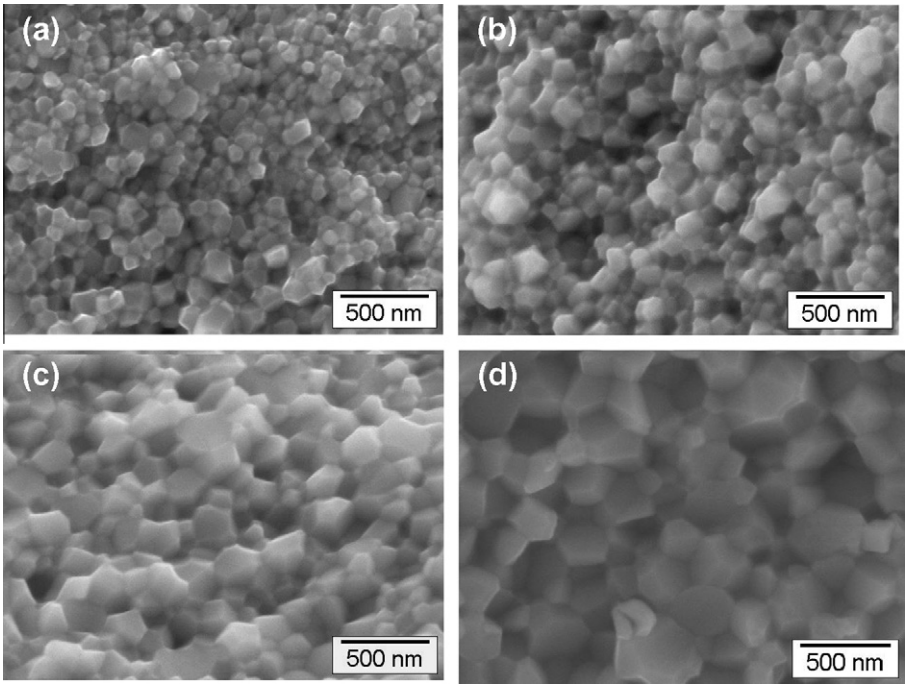

Fig. 12. SEM images of fracture surfaces of CeO_2 sintered for different holding times: (a) 0, (b) 2 (c) 5, and (d) 7 min (temperature: 780 °C; pressure: 400 MPa; heating rate: 140 °C min^{-1}).

ates) and it can also have an intrinsic effect, by a change in the chemical potential and through plastic flow. The presence of agglomerates in nanopowders is a common occurrence and has been identified as an important cause of the difficulty in sintering these powders to high densities at relatively low temperatures. The nature of these agglomerates (soft or hard) is dictated by the type of bond between grains: van der Waals in soft agglomerates and solid necks in hard agglomerates, the latter may form during subsequent processing, e.g., calcination. In a recent publication, Balakrishnan et al. [23] showed that agglomerates made of nanograins exhibit higher strength than those made of micrometric grains. From a simulation of uniaxial compaction they demonstrated that adhesion forces between grains are responsible for the commonly observed difficulty in compacting nanopowders and for the nonuniformity in microstructure in the powders prior to consolidation.

The effect of pressure on grain size for samples sintered in the range 650–700 °C is also shown in Fig. 7. Relatively small changes in grain size are seen, with the size increasing by less than a factor of two. At the highest sintering temperature (700 °C), the samples were still nanometric with a grain size of about 70 nm. SEM images, Fig. 8, also show no significant increase in grain size with an increase in pressure.

The effect of heating rate on densification and grain growth for sintering at 780 °C with zero hold time is shown in Fig. 9. As the heating rate was increased from 90 to 330 °C min^{-1} the density showed no change. Similarly, the heating rate had a relatively small effect on grain size, decreasing it from 113 to 88 nm over the range of heating rate investigated. The SEM images of samples sintered at different heating rates are shown in Fig. 10. It should be noted that, expectedly, the grain size of samples sintered at this temperature (780 °C) is much larger than that for samples sintered at 700 °C. Thus the heating rate has an effect on grain growth, albeit not large.

The work of Shen et al. [24] on alumina showed that heating rate had little effect on the density up to a value of about 350 °C min^{-1} and then had a negative effect on the final density with higher heating rates (the density decreased as the rate increased up to 600 °C min^{-1}). The grain size, however, showed a dependence which was strongest at lower heating rates (the grain size decrease was significant as the heating rate increased between 50 and 200 °C min^{-1}).

Fig. 11 shows the relative density and grain size of ceria as functions of holding time. All relative densities exceeded 98% for all holding times, increasing only by a small amount as the holding time is increased from 0 to 10 min. The behavior of grain size, however, was different, remaining constant for times of up to 2 min (with a value of about 100 nm) then increasing significantly for holding times up to 10 min to 260 nm. Fig. 12 shows SEM images of fracture surfaces of sintered samples with different holding time. As can be seen from these images, little change takes place between 0 and 2 min and then grain size increases significantly at longer holding times. These observations indicate that during the first 2 min, densification took place with no grain growth; grain growth was most evident for holding times between 5 and 10 min. The interpretation of these results focuses on the presence of porosity. During the initial 2 min, when the density is ~99% or less, pores act to retard grain growth, as has been observed by Marder et al. [25] on their investigation on the sintering of nanometric Y_2O_3 (18 nm) powders under SPS conditions at 1100 °C. This conclusion was validated by theoretical calculations on grain growth. That isolated nanopores exist at grain boundaries has been demonstrated by TEM observations on densified nanostructured oxides, including cubic yttria-stablized zirconia [25–27]. When the density increases to near theoretical value, the concentration of pores becomes exceedingly small and their role in grain growth retardation becomes insignificant. At this point, grain growth becomes active, as we believe is the reason for the increase in grain size after the 2-min sintering time, as seen in Fig. 12.

4. Conclusions

The sintering behavior of ceria ceramics with nano-sized grains was investigated systematically as a function of the spark plasma

sintering (SPS) parameters of temperature, applied pressure, heating rate, and holding time. Ceria could be consolidated to a relative density above 97% with nano-grains at a temperature as low as 650 °C under high pressure (500 MPa), high heating rate (130 °C min^{-1}), and short holding time (5 min). The high applied pressure and fast heating rate promoted densification of CeO_2 ceramics at much lower temperature for very short holding time with very limited grain growth. Furthermore, the results show that control of microstructure with a desired the grain size is possible through proper choice of SPS parameters.

Acknowledgments

Financial support for this project was provided by the Department of Energy (DOE) and by Idaho National laboratory.

References

[1] H. Yahieo, Y. Baba, K. Egneli, H. Arai, J. Electrochem. Soc. 135 (1988) 2077.
[2] P. Jasinski, T. Suzuki, H.U. Anderson, Sens. Actuators B 95 (2003) 73.
[3] G. RangaRao, P. Fornasiero, R. Dimonte, J. Kaspar, G. Vlaic, G. Balducci, S. Meriani, A. Gubitosa, M. Cremona, M. Graziani, J. Catal. 162 (1996) 1.
[4] A. Morikkawa, T. Suzuki, T. Kanazawa, K. Kikuta, A. Suda, H. Shinjo, Appl. Catal. B 78 (2008) 210.
[5] H.S. Kim, C.Y. Joung, B.H. Lee, J.Y. Oh, Y.H. Koo, P. Heimgartner, J. Nucl. Mater. 378 (2008) 98.
[6] R.C. O'Brien, R.M. Ambrosi, N.P. Bannister, S.D. Howe, H.V. Atkinson, J. Nucl. Mater. 393 (2009) 108.
[7] T. Sonoda, M. Kinoshita, Y. Chimi, N. Ishikawa, M. Sataka, A. Iwase, Nucl. Instrum. Methods Phys. B 250 (2006) 254.
[8] P.L. Chen, I.W. Chen, J. Am. Ceram. Soc. 76 (1993) 1577.
[9] Y. Zhou, R.J. Phillips, J.A. Switzer, J. Am. Ceram. Soc. 78 (1995) 981.
[10] P. Duran, F. Capel, D. Guitierrez, J. Tartaj, C. Moure, J. Eur. Ceram. Soc. 22 (2002) 1711.
[11] Y. Kinemuchi, K. Watari, J. Eur. Ceram. Soc. 28 (2008) 2019.
[12] Y. Zhou, M.N. Rahaman, Acta Mater. 45 (1997) 3635.
[13] M. Ozawa, Scripta Mater. 50 (2004) 61.
[14] H.C. Yao, Y.F. YuYao, J. Catal. 86 (1984) 254.
[15] S.K. Tadokoro, T.C. Porfirio, R. Mucillo, E.N.S. Mucillo, J. Power Sources 130 (2004) 15.
[16] P. Duran, C. Moure, J.R. Jurado, J. Mater. Sci. 29 (1994) 1940.
[17] T. Mori, T. Kobayashi, Y. Wang, J. Drennan, T. Nishimura, J.G. Li, H. Kobayashi, J. Am. Ceram. Soc. 88 (2005) 1981.
[18] U. Anselmi-Tamburini, J.E. Garay, Z.A. Munir, Scripta Mater. 54 (2006) 823.
[19] Z.A. Munir, U. Anselmi-Tamburini, M. Ohyanagi, J. Mater. Sci. 41 (2006) 763.
[20] O.M. Lemine, Superlattices Microstruct. 45 (2009) 576.
[21] R.M. German, Sintering Theory and Practice, Wiley, New York, 1996, p. 482.
[22] R.M. German, Sintering Theory and Practices, Wiley, New York, 1996, p. 170.
[23] A. Balakrishnan, P. Pizette, C.L. Martin, S.V. Joshi, B.P. Saha, Acta Mater. 58 (2010) 802.
[24] Z. Shen, M. Johnsson, Z. Zhao, M. Nygren, J. Am. Ceram. Soc. 85 (2002) 1921.
[25] R. Marder, R. Chaim, C. Estournes, Mater. Sci. Eng. A 527 (2010) 1577.
[26] U. Anselmi-Tamburini, J.N. Woolman, Z.A. Munir, Adv. Funct. Mater. 17 (2007) 3267.
[27] B.N. Kim, K. Hiraga, K. Morita, H. Yoshida, T. Miyazaki, Y. Kagawa, Acta Mater. 57 (2009) 1319.